

Article

Simultaneous Generation of Two Orthogonally Polarized Terahertz Waves by Stimulated Polariton Scattering with a Periodically Poled LiNbO₃ Crystal

Zhongyang Li * , Silei Wang, Mengtao Wang, Bin Yuan and Pibin Bing 

College of Electric Power, North China University of Water Resources and Electric Power, Zhengzhou 450045, China; 201610521173@stu.ncwu.edu.cn (S.W.); 201610521175@stu.ncwu.edu.cn (M.W.); x201710518296@stu.ncwu.edu.cn (B.Y.); bing463233@163.com (P.B.)

* Correspondence: thzwave@163.com; Tel.: +86-158-3827-6960

Received: 7 April 2018; Accepted: 20 July 2018; Published: 24 July 2018



Abstract: We present a theoretical investigation of the simultaneous generation of two orthogonally polarized terahertz (THz) waves by stimulated polariton scattering (SPS) with a periodically poled LiNbO₃ (PPLN) crystal. The two orthogonally polarized THz waves are generated from SPS with A_1 and E symmetric transverse optical (TO) modes in a LiNbO₃ crystal, respectively. The parallel polarized THz wave is generated from A_1 symmetric TO modes with type-0 phase-matching of $e = e + e$, and the perpendicular polarized THz wave is generated from E symmetric TO modes with type-I phase-matching of $e = o + o$. The two types of phase-matching of $e = e + e$ and $e = o + o$ can be almost satisfied simultaneously by accurately selecting the poling period of the PPLN crystal. We calculate the photon flux density of the two orthogonally polarized THz waves by solving the coupled wave equations. The calculation results indicate that the two orthogonally polarized THz waves can be efficiently generated, and the relative intensities between the two orthogonally polarized THz waves can be modulated.

Keywords: terahertz wave; stimulated polariton scattering; periodically poled LiNbO₃

1. Introduction

Stimulated polariton scattering (SPS) has proven to be an efficient scheme to generate terahertz (THz) waves [1–8]. A polariton is a coupled quantum between the pump laser and the infrared- and Raman-active transverse optical (TO) modes in a crystal, and it behaves like phonons near the resonant frequency associated with the TO mode and exhibits photon-like behavior for lower non-resonant frequencies [1]. SPS consists of second-order and third-order nonlinear frequency conversion processes where a pump photon stimulates a Stokes photon at the difference frequency between the pump photon and the polariton. At the same time, a THz wave is generated by the parametric process due to the nonlinearity arising from both electronic and vibrational contributions of the crystal. The TO phonon resonances can contribute substantially to the magnitude of the second- and third-order nonlinearities, which are beneficial to the THz generation via SPS.

MgO:LiNbO₃ has been the most widely used crystal for THz wave generation via SPS [1–5]. MgO:LiNbO₃ has strong second-order nonlinear response, as well as TO phonon resonances for efficient SPS [9]. MgO:LiNbO₃ has five A_1 symmetric infrared- and Raman-active TO modes polarized parallel to the c -axis with frequencies of 248 cm⁻¹, 274 cm⁻¹, 307 cm⁻¹, 628 cm⁻¹, and 692 cm⁻¹ [10]. MgO:LiNbO₃ has eight E symmetric infrared- and Raman-active TO modes polarized perpendicular to the c -axis with frequencies of 152 cm⁻¹, 236 cm⁻¹, 265 cm⁻¹, 322 cm⁻¹, 363 cm⁻¹, 431 cm⁻¹, 586 cm⁻¹, and 670 cm⁻¹ [10]. A_1 symmetric TO modes have been the most widely used for THz wave generation

via SPS [1–5]. However, E symmetric TO modes can be also employed to generate THz waves via SPS. In 1969, Yarborough reported the observation of tunable SPS from A_1 and E symmetric TO modes with a pump wave in a LiNbO_3 crystal [11]. If the SPS from A_1 and E symmetric TO modes can be simultaneously excited, then two orthogonally polarized THz waves can be simultaneously generated. Orthogonally polarized THz waves are useful for imaging [12]. Yu et al. [12] showed that the addition or subtraction of two images, which were taken with a perpendicularly polarized THz wave and parallel polarized THz wave, was effective to enhance the contrast of terahertz images.

In this work, we theoretically study the simultaneous generation of two orthogonally polarized THz waves by SPS with a periodically poled LiNbO_3 (PPLN) crystal. The two orthogonally polarized THz waves are generated from SPS with A_1 and E symmetric TO modes in a $\text{MgO}:\text{LiNbO}_3$ crystal, respectively. We calculate the photon flux density of the two orthogonally polarized THz waves by solving the coupled wave equations.

2. Theoretical Model

Figure 1 shows a schematic diagram of THz wave generation by the SPS processes by a PPLN crystal with a quasi-phase-matching (QPM) condition. A pump wave and two seed waves (Seed_e and Seed_o) propagate along the x -axis of the PPLN crystal. The electric field of the pump wave and Seed_e is along the z -axis of the PPLN crystal, whereas the electric field of Seed_o is perpendicular to the z -axis of the PPLN crystal. The z -axis is the optical axis of the LiNbO_3 crystal. The poling period of the PPLN crystal is Λ . Two orthogonally polarized THz waves (THz_e and THz_o) are generated by the SPS processes. The electric field of THz_e is along the z -axis of the PPLN crystal, whereas the electric field of THz_o is perpendicular to the z -axis of the PPLN crystal. The pump, Seed_e , and THz_e waves satisfy the type-0 phase-matching of $e = e + e$, whereas the pump, Seed_o , and THz_o waves satisfy the type-I phase-matching of $e = o + o$. The above two types of phase-matching can also be applied to the forward SPS processes and backward SPS processes by accurately selecting the poling period Λ of the PPLN crystal. The generated THz waves are deflected by parabolic mirrors, which transmit the pump and two seed waves.

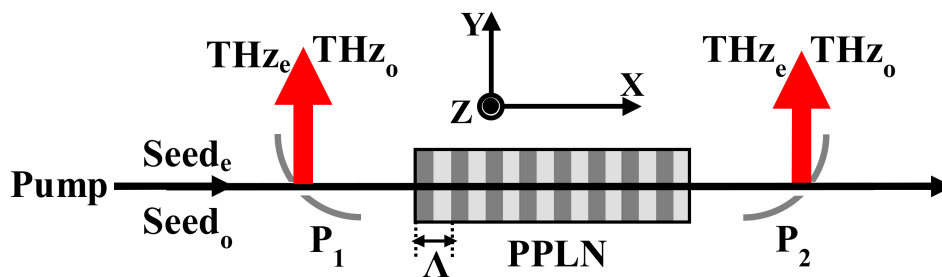


Figure 1. Schematic diagram of terahertz (THz) wave generation by stimulated polariton scattering (SPS) processes in a periodically poled LiNbO_3 (PPLN) crystal with a quasi-phase-matching (QPM) condition. Λ is the poling period of the PPLN crystal. P_1 and P_2 are parabolic mirrors which transmit the pump and two seed waves, and couple out the two THz waves.

3. Phase-Matching Characteristics

Due to the different eigenfrequency, oscillator strength, and bandwidth of the TO modes, the two orthogonally polarized THz waves, THz_e and THz_o , have different dispersion and absorption characteristics. Figure 2 shows the dispersion and absorption characteristics of the THz_e and THz_o waves. n_{Te} and n_{To} are the refractive indices of THz_e and THz_o , respectively, and α_{Te} and α_{To} are the absorption coefficients of THz_e and THz_o , respectively. The curves of n_{Te} and α_{Te} are below the lowest A_1 symmetric TO mode, 248 cm^{-1} , and the curves of n_{To} and α_{To} are below the lowest E symmetric TO mode, 152 cm^{-1} . The theoretical parameters of the refractive index and absorption coefficient for LiNbO_3 in the THz range are cited in [9]. From the figure, we find that n_{Te} and n_{To} are larger than 5.

The value of the refractive index in the THz range is much larger than that in the optical range, so the collinear phase-matching is impossible to realize. The absorption coefficients α_{Te} and α_{To} are very large, especially in the high THz frequency range.

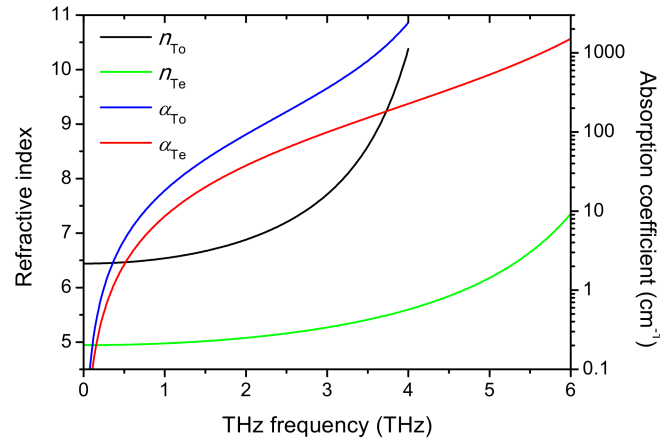


Figure 2. The dispersion and absorption characteristics of the two orthogonally polarized THz waves, THZ_e and THZ_o. n_{Te} and n_{To} are the refractive indices of THZ_e and THZ_o, respectively, and α_{Te} and α_{To} are the absorption coefficient of THZ_e and THZ_o, respectively.

In the optical SPS processes, the THz waves are generated, and the seed waves are amplified. The amplified seed waves are Stokes waves. In order to achieve efficient conversion of the SPS processes from the pump wave to the THz waves, a precise phase-matching condition must be satisfied. For the forward SPS processes, the pump, Seed_e, and THZ_e waves satisfy the type-0 phase-matching of $e = e + e$, and the phase mismatch Δk_e is as follows:

$$\vec{\Delta k}_e = \vec{k}_p - \vec{k}_{se} - \vec{k}_{Te} + \vec{k}_\Lambda. \tag{1}$$

The pump, Seed_o, and THZ_o waves satisfy the type-I phase-matching of $e = o + o$, and the phase mismatch Δk_o is as follows:

$$\vec{\Delta k}_o = \vec{k}_p - \vec{k}_{so} - \vec{k}_{To} + \vec{k}_\Lambda \tag{2}$$

where \vec{k}_p is the wave vector of the pump wave, \vec{k}_{se} and \vec{k}_{so} are the wave vectors of the two Seed_e and Seed_o waves, respectively, and \vec{k}_{Te} \vec{k}_{To} are the wave vectors of the two THZ_e and THZ_o waves, respectively. $\vec{k}_\Lambda = 2\pi/\Lambda$ is the grating vector, and Λ is the poling period of the PPLN crystal.

For the backward SPS processes, the pump, Seed_e and THZ_e waves satisfy the type-0 phase-matching of $e = e + e$, and the phase mismatch Δk_e is as follows:

$$\vec{\Delta k}_e = \vec{k}_p - \vec{k}_{se} + \vec{k}_{Te} - \vec{k}_\Lambda. \tag{3}$$

The pump, seed_o, and THZ_o waves satisfy the type-I phase-matching of $e = o + o$, and the phase mismatch Δk_o is as follows:

$$\vec{\Delta k}_o = \vec{k}_p - \vec{k}_{so} + \vec{k}_{To} - \vec{k}_\Lambda. \tag{4}$$

The energy conservation condition has to be fulfilled according to the following:

$$\frac{1}{\lambda_p} - \frac{1}{\lambda_{se}} - \frac{1}{\lambda_{Te}} = 0 \tag{5}$$

$$\frac{1}{\lambda_p} - \frac{1}{\lambda_{s_e}} - \frac{1}{\lambda_{T_e}} = 0 \quad (6)$$

where λ_p is the wavelength of pump wave, λ_{s_e} and λ_{s_o} are the wavelengths of the two Seed_e and Seed_o waves, respectively, and λ_{T_e} λ_{T_o} are the wavelengths of the two THz_e and THz_o waves, respectively. If both the phase mismatches Δk_e and Δk_o are small enough, two perpendicular THz waves THz_e and THz_o can be generated simultaneously with a single pump wave.

For the SPS processes, we calculate the phase mismatches Δk_e and Δk_o according to Equations (1) and (2), respectively, at a fixed pump wavelength. The wavelengths of the two seed waves and the two THz waves are dependent on Equations (5) and (6). The sum phase mismatch $\Delta k_s = \left| \Delta k_e \right| + \left| \Delta k_o \right|$. If the sum phase mismatch Δk_s is small enough, the two phase mismatches Δk_e and Δk_o are small enough to realize the two phase-matching conditions of $e = e + e$ and $e = o + o$.

Figure 3 shows the phase-matching characteristics for the forward SPS processes with a pump wavelength of 1550 nm. ν_{T_e} and ν_{T_o} are the frequencies of the THz_e and THz_o waves, respectively. The theoretical values of the refractive indices are calculated using a Sellmeier equation for LiNbO₃ in the infrared range [13]. From Figure 3a, we find that as Λ varies from 9 to 18 μm , there are many points of Δk_s with values below $\pi \text{ cm}^{-1}$, which indicates that the two SPS processes generating the THz_e and THz_o waves can be efficiently realized. Most frequencies from 4.6 to 6 THz of THz_e and most frequencies from 0.4 to 2.8 THz of THz_o can be efficiently generated. The minimum value of Δk_s is 0.064 cm^{-1} with Λ of 17.1 μm , corresponding to ν_{T_e} of 4.66 THz and ν_{T_o} of 0.56 THz. Figure 3b shows the detailed phase-matching characteristics with Λ from 17.096 to 17.100 μm . As Λ varies from 17.0981 to 17.0983 μm , Δk_s with a value of 0.0369 cm^{-1} is small enough to stimulate the two SPS processes. In particular, as Λ is 17.0982 μm , Δk_e equals Δk_o , which indicates that the two SPS processes can be realized to equal degrees.

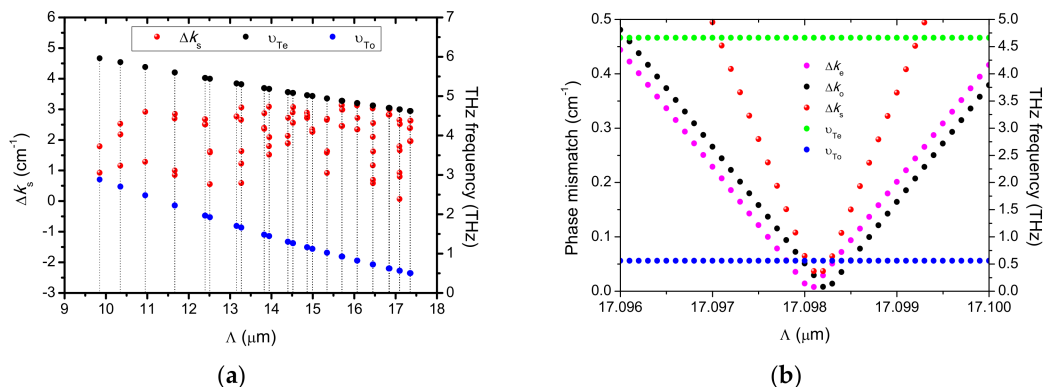


Figure 3. The phase-matching characteristics for the forward SPS processes. ν_{T_e} and ν_{T_o} are the frequencies of the THz_e and THz_o waves, respectively. The sum phase mismatch $\Delta k_s = \left| \Delta k_e \right| + \left| \Delta k_o \right|$, and $\lambda_p = 1550 \text{ nm}$. (a) The phase-matching characteristics with Λ from 9 to 18 μm . (b) The detailed phase-matching characteristics with Λ from 17.096 to 17.100 μm .

Figure 4 shows the phase-matching characteristics for the backward SPS processes with a pump wavelength of 1550 nm. From Figure 4a, we find that as Λ varies from 20 to 100 μm , there are also many points of Δk_s with values below $\pi \text{ cm}^{-1}$, particularly below 1 cm^{-1} . Most frequencies from 0.45 to 2.03 THz of THz_e and most frequencies from 2.01 to 3 THz of THz_o can be efficiently generated. The minimum value of Δk_s is 0.344 cm^{-1} with Λ of 80.98 μm , corresponding to ν_{T_e} of 0.52 THz and ν_{T_o} of 2.06 THz. Figure 4b shows the detailed phase-matching characteristics with Λ around 80.98 μm . As Λ varies from 80.960 to 80.995 μm , Δk_s with a value of 0.344 cm^{-1} is small enough to stimulate the

two SPS processes. In particular, as Λ is 80.978 μm , Δk_e equals Δk_o , which indicates that the two SPS processes can be realized to equal degrees.

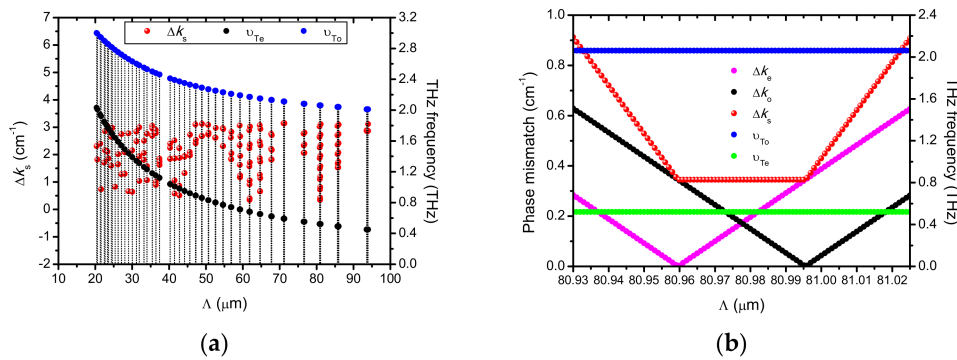


Figure 4. The phase-matching characteristics for the backward SPS processes, $\lambda_p = 1550$ nm. (a) The phase-matching characteristics with Λ from 20 to 100 μm . (b) The detailed phase-matching characteristics with Λ from 80.93 to 81.02 μm .

4. THz Photon Flux Density

The coupled wave equations for the SPS processes can be found in [9,14]. The coupled wave equations describe the field envelope variation of the pump, Stokes, and THz waves. The analytical expression of THz parametric gain coefficient g_T under the QPM condition in the international system of units can be written as follows:

$$g_T = \frac{\alpha_T}{2} \left\{ \left[1 + 16 \cos^2 \varphi \left(\frac{g_0}{\alpha_T} \right)^2 \right]^{\frac{1}{2}} - 1 \right\} \quad (7)$$

$$g_0^2 = \frac{\omega_s \omega_T}{128 \pi^2 \epsilon_0 c^3 n_p n_s n_T} I_p \left(d_E + \sum_j \frac{S_j \omega_{0j}^2 d_{Qj}}{\omega_{0j}^2 - \omega_T^2} \right)^2 \quad (8)$$

$$\alpha_T = 2 \frac{\omega_T}{c} \text{Im} \left(\epsilon_\infty + \sum_j \frac{S_j \omega_{0j}^2}{\omega_{0j}^2 - \omega_T^2 - i \omega_T \Gamma_j} \right)^{\frac{1}{2}} \quad (9)$$

where ω_{0j} , S_j , and Γ_j denote the eigenfrequency, the oscillator strength of the polariton modes, and the bandwidth of the j th TO mode in the LiNbO₃ crystal, respectively. I_p is the power density of the pump wave, and g_0 is the low-loss parametric gain. n_p , n_s , and n_T are the refractive indices of the pump, Stokes, and THz waves, respectively. φ is the angle between the wavevectors of the pump wave and THz wave. α_T is material absorption coefficient in THz region. d_E and d_Q are nonlinear coefficients related to pure parametric (second-order) and Raman (third-order) scattering processes, respectively.

When THz frequencies are far below the lowest A_1 symmetry TO mode of 248 cm^{-1} and the lowest E symmetry TO mode of 152 cm^{-1} , Equation (8) can be rewritten as follows [9]:

$$g_0^2 = \frac{\omega_s \omega_T}{128 \pi^2 \epsilon_0 c^3 n_p n_s n_T} I_p \left(d_E + \sum_j S_j d_{Qj} \right)^2. \quad (10)$$

For SPS with type-0 phase-matching of $e = e + e$, the relationship between d_E and d_Q is given by [9,15,16] the following:

$$d_E + \sum_j S_j d_{Qj} = \frac{1}{4} r_{33} n_p^4. \quad (11)$$

For SPS with type-I phase-matching of $e = o + o$, the relationship between d_E and d_Q is as follows:

$$d_E + \sum_j S_j d_{Q_j} = \frac{1}{4} r_{13} n_p^4 \quad (12)$$

where r_{33} and r_{13} are the linear electro-optic coefficients of LiNbO₃.

With strong THz wave absorption and phase mismatch and without pump depletion, the coupled wave equations can be solved to give the THz photon flux density ϕ_T with a general solution [17], given by the following:

$$\phi_T = \phi_s(0) e^{-\alpha_T L/2} \frac{g_T^2}{g_T^2 + \left(\frac{\alpha_T}{4} - j\frac{\Delta k}{2}\right)^2} \times \left| \sinh \left(\sqrt{g_T^2 + \left(\frac{\alpha_T}{4}\right)^2} L \right) \right|^2 \quad (13)$$

where Δk is the phase mismatching and L is the crystal length. The initial THz photon flux density ϕ_T is assumed to be zero, and $\phi_s(0)$ is the initial seed wave photon flux density. The initial photon flux densities of Seed_e and seed_o are $\phi_{se}(0)$ and $\phi_{so}(0)$, respectively. The THz photon flux densities of THz_e and THz_o are ϕ_{Te} and ϕ_{To} , respectively. The ratio R of $\phi_{so}(0)$ to $\phi_{se}(0)$ is as follows:

$$R = \frac{\phi_{so}(0)}{\phi_{se}(0)}. \quad (14)$$

Figure 5 shows the THz wave photon flux densities ϕ_{Te} and ϕ_{To} for the forward SPS processes. From Figure 5a–d, we find that when Λ varies from 15 to 19 μm , ϕ_{Te} and ϕ_{To} increase first and then decrease. When Λ is equal to 17.0982 μm , ϕ_{Te} and ϕ_{To} reach their maximum values as the phase mismatches Δk_e and Δk_o reach their minimum values. The maximum value of ϕ_{Te} is $5.74 \times 10^{-6} \text{ s}^{-1} \text{ cm}^{-2}$. The value of ϕ_{Te} is so small, because the THz absorption coefficient of 4.66 THz is very large. ϕ_{To} increases with the increase of R . The relative photon flux densities between ϕ_{Te} and ϕ_{To} can be tuned by varying R . When R is 0.0037, the maximum values of ϕ_{Te} and ϕ_{To} are approximately equal. From Figure 5e, we find that when crystal length L varies from 0 to 30 mm, ϕ_{Te} and ϕ_{To} increase rapidly and smoothly. When R is 0.00323, the values of ϕ_{Te} and ϕ_{To} are approximately equal, as L is larger than 20 mm.

Figure 6 shows the THz wave photon flux densities ϕ_{Te} and ϕ_{To} for the backward SPS processes. From Figure 6a, we find that when Λ varies from 74 to 88 μm , ϕ_{Te} and ϕ_{To} increase first and then decrease. When Λ is equal to 80.978 μm , ϕ_{Te} and ϕ_{To} reach their maximum values as the phase mismatches Δk_e and Δk_o reach their minimum values. The maximum value of ϕ_{Te} is $43.62 \text{ s}^{-1} \text{ cm}^{-2}$. The maximum value of ϕ_{Te} in the backward SPS processes is larger than that in the forward SPS processes, because the THz absorption coefficient of 0.52 THz in the backward SPS processes is smaller than that of 4.66 THz in the forward SPS processes. The relative photon flux densities between ϕ_{Te} and ϕ_{To} can be tuned by varying R . When R is 2.5×10^7 , the maximum values of ϕ_{Te} and ϕ_{To} are approximately equal. From Figure 6b, we find that when crystal length L varies from 0 to 50 mm, ϕ_{Te} and ϕ_{To} increase rapidly and smoothly. When R is 5.21×10^7 and L is larger than 40 mm, the values of ϕ_{Te} and ϕ_{To} are approximately equal.

The intensities of generated THz waves are very low, because the THz waves are heavily absorbed by the PPLN crystal. However, the intensities of the THz waves can be enhanced by injection intense seed waves, as shown in Equation (13). Moreover, one can use organic crystals with QPM, because organic crystals have larger nonlinear optical coefficients and lower absorption coefficients in the THz region [18]. Furthermore, the enhancement of the THz intensities can be realized by cryogenic cooling. At liquid nitrogen temperature, the gain coefficients of the THz waves in the SPS processes are enhanced. At the same time, the absorption coefficients of the THz waves decrease.

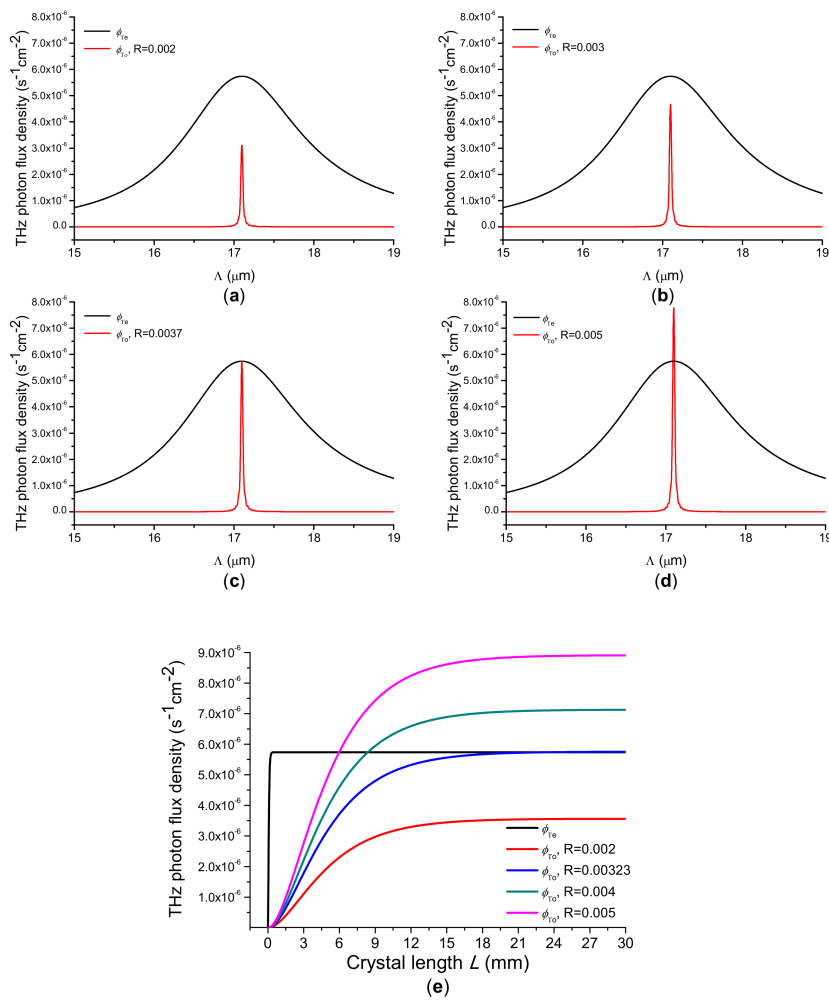


Figure 5. THz wave photon flux density ϕ_T for the forward SPS processes. $\lambda_p = 1550$ nm, $\nu_{Te} = 4.66$ THz, $\nu_{T0} = 0.56$ THz, $I_p = 100$ MW/cm², and $\phi_{se}(0) = 10^6$ s⁻¹cm⁻². (a–d) ϕ_T versus Λ with $R = 0.002$, 0.003, 0.0037, and 0.005, respectively. $L = 10$ mm. (e) ϕ_T versus crystal length L . $\Lambda = 17.0982$ μm .

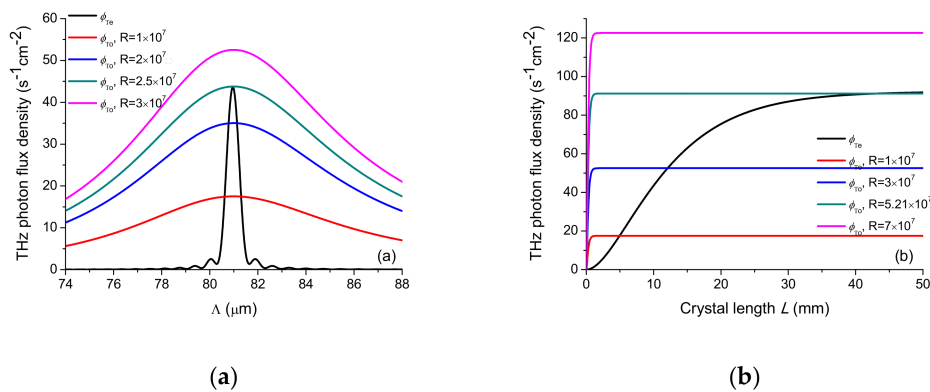


Figure 6. THz wave photon flux density ϕ_T for the backward SPS processes. $\lambda_p = 1550$ nm, $\nu_{Te} = 0.52$ THz, $\nu_{T0} = 2.06$ THz, $I_p = 100$ MW/cm², and $\phi_{se}(0) = 10^6$ s⁻¹cm⁻². (a) ϕ_T versus Λ from 74 to 88 μm . $L = 10$ mm. (b) ϕ_T versus crystal length L . $\Lambda = 80.978$ μm .

The scheme in this work of generating two orthogonally polarized THz waves by SPS processes has certain advantages. First of all, the two orthogonally polarized THz waves are simultaneously

generated by a pump wave, which means that the two THz waves are phase-conjugate. Second, the two orthogonally polarized THz waves are generated only by a PPLN crystal. Third, the intensities of the two orthogonally polarized THz waves can be tuned by varying the intensities of the input seed waves.

5. Conclusions

We present the simultaneous generation of two orthogonally polarized THz waves by forward and backward SPS processes with a PPLN crystal. The minimum values of Δk_s of 0.064 cm^{-1} in the forward SPS processes and 0.344 cm^{-1} in the backward SPS processes indicate that the type-0 phase-matching generating parallel polarized THz wave and the type-I phase-matching generating perpendicular polarized THz wave can almost be satisfied simultaneously. In particular, the two SPS processes can be excited to equal degrees by accurately selecting the poling period of the PPLN crystal. We calculate the photon flux densities of the two orthogonally polarized THz waves by solving the coupled wave equations. The theoretical calculations show that the photon flux densities of the two orthogonally polarized THz waves are very small. The relative intensities between the two orthogonally polarized THz waves can be modulated by varying the intensities of the input seed waves.

Author Contributions: Z.L., S.W., and M.W. conceived of the original idea; B.Y. and P.B. contributed useful and deep discussions; and Z.L. wrote the manuscript. All authors read and approved the final version of the manuscript.

Funding: This work was supported by the National Natural Science Foundation of China (61601183); the Natural Science Foundation of Henan Province (162300410190); the Program for Innovative Talents (in Science and Technology) in University of Henan Province (18HASTIT023); the Young Backbone Teachers in University of Henan Province (2014GGJS-065); and the Program for Innovative Research Team (in Science and Technology) in University of Henan Province (16IRTSTHN017).

Conflicts of Interest: All contributing authors declare no conflicts of interest. The founding sponsors had no role in the design of the study; in the collection, analyses, or interpretation of the data; in the writing of the manuscript; or in the decision to publish the results.

References

1. Kawase, K.; Shikata, J.; Ito, H. Terahertz wave parametric source. *J. Phys. D Appl. Phys.* **2002**, *35*, R1–R14. [[CrossRef](#)]
2. Ikari, T.; Guo, R.; Minamide, H.; Ito, H. Energy scalable terahertz-wave parametric oscillator using surface-emitted configuration. *J. Eur. Opt. Soc.-Rapid Publ.* **2010**, *5*, 10054.
3. Ortega, T.A.; Pask, H.M.; Spence, D.J.; Lee, A.J. THz polariton laser using an intracavity Mg:LiNbO₃ crystal with protective Teflon coating. *Opt. Express* **2017**, *25*, 3991–3999. [[CrossRef](#)] [[PubMed](#)]
4. Zhang, R.; Qu, Y.; Zhao, W.; Chen, Z. High energy, widely tunable Si-prism-array coupled terahertz-wave parametric oscillator with a deformed pump and optimal crystal location for angle tuning. *Appl. Opt.* **2017**, *56*, 2412–2417. [[CrossRef](#)] [[PubMed](#)]
5. Molter, D.; Theuer, M.; Beigang, R. Nanosecond terahertz optical parametric oscillator with a novel quasi-phase-matching scheme in lithium niobate. *Opt. Express* **2009**, *17*, 6623–6628. [[CrossRef](#)] [[PubMed](#)]
6. Jang, H.; Strömqvist, G.; Pasiskevicius, V.; Canalias, C. Control of forward stimulated polariton scattering in periodically-poled KTP crystals. *Opt. Express* **2013**, *21*, 27277–27283. [[CrossRef](#)] [[PubMed](#)]
7. Jang, H.; Viotti, A.; Strömqvist, G.; Zukauskas, A.; Canalias, C.; Pasiskevicius, V. Counter-propagating parametric interaction with phonon-polaritons in periodically poled KTiOPO₄. *Opt. Express* **2017**, *25*, 2677–2686. [[CrossRef](#)] [[PubMed](#)]
8. Wu, M.; Chiu, Y.; Wang, T.; Zhao, G.; Zukauskas, A.; Laurell, F.; Huang, Y. Terahertz parametric generation and amplification from potassium titanyl phosphate in comparison with lithium niobate and lithium tantalate. *Opt. Express* **2016**, *24*, 25964–25973. [[CrossRef](#)] [[PubMed](#)]
9. Sussman, S.S. *Tunable Light Scattering from Transverse Optical Modes in Lithium Niobate*; Microwave Laboratory Report 1970, No. 1851; Stanford University: Stanford, CA, USA, 1970.
10. Barker, A.S., Jr.; Ballman, A.A.; Ditzenberger, J.A. Infrared study of the lattice vibrations in LiNbO₃. *Phys. Rev. B* **1970**, *2*, 4233–4239. [[CrossRef](#)]

11. Gelbwachs, J.; Pantell, R.H.; Puthoff, H.E.; Yarborough, M.J. A tunable stimulated Raman oscillator. *Appl. Phys. Lett.* **1969**, *14*, 258–262. [[CrossRef](#)]
12. Yu, X.; Endo, M.; Ishibashi, T.; Shimizu, M.; Kusanagi, S.; Nozokido, T.; Bae, J. Orthogonally polarized terahertz wave imaging with real-time capability for food inspection. In Proceedings of the IEEE Microwave Conference (APMC), Nanjing, China, 6–9 December 2015; Volume 2, pp. 1–3.
13. Dolev, I.; Ganany-Padowicz, A.; Gayer, O.; Arie, A.; Mangin, J.; Gadret, G. Linera and nonlinear optical properties of MgO:LiNbO₃. *Appl. Phys. B* **2009**, *96*, 423–432. [[CrossRef](#)]
14. Walsh, D.A. Intracavity Terahertz Optical Parametric Oscillators. Doctoral Dissertation, University of St Andrews, St Andrews, Scotland, 2011.
15. Yariv, A. *Quantum Electronics*, 3rd ed.; Wiley: New York, NY, USA, 1988; Chapter 16.
16. Johnston, W.D.; Kaminow, I.P. Contributions to Optical Nonlinearity in GaAs as Determined from Raman Scattering Efficiencies. *Phys. Rev.* **1969**, *188*, 1209–1211. [[CrossRef](#)]
17. Kitaeva, G.K.; Penin, A.N. Parametric frequency conversion in layered nonlinear media. *J. Exp. Theor. Phys.* **2004**, *98*, 272–286. [[CrossRef](#)]
18. Majkić, A.; Zgonik, M.; Petelin, A.; Jazbinšek, M.; Ruiz, B.; Medrano, C.; Günter, P. Terahertz source at 9.4 THz based on a dual-wavelength infrared laser and quasi-phase matching in organic crystals OH1. *Appl. Phys. Lett.* **2014**, *105*, 141115. [[CrossRef](#)]



© 2018 by the authors. Licensee MDPI, Basel, Switzerland. This article is an open access article distributed under the terms and conditions of the Creative Commons Attribution (CC BY) license (<http://creativecommons.org/licenses/by/4.0/>).